Team Desciption paper: BabyTigers - R 2024

Shohei Yasuda, Kosuke Nakajima, Ryota Tanabe, and Wataru Uemura[0000−0001−6012−0029]

Ryukoku University, 1-5, Seta Ohe, Otsu City, Shiga, Japan
robocup@vega.elec.ryukoku.ac.jp, wataru@rins.ryukoku.ac.jp
https://vega.elec.ryukoku.ac.jp/trac/wiki/BabyTigers-R

Abstract. This paper presents Baby-Tigers-R[1], a team comprising members from Electronics, information and communication engineering course, Faculty of advanced science and technology at Ryukoku University.
Within our laboratory, we are actively engaged in research concerning autonomous mobile robots and visible light communication. The collaboration of autonomous mobile robots holds significant importance, particularly in the evolving landscape of factory production, transitioning from low-mix mass production to high-mix low-volume production. Our research focuses on exploring criteria for computer selection in autonomous mobile robots, pathfinding algorithms, and marker recognition techniques.

Keywords: Logistics League, RoboCup, BabyTigers - R, robotino, autonomous mobile robot.

1 Introcution

This paper introduces Baby-Tigers-R, which is a team consisted of members belonging to Electronics, Information and communication engineering course, Faculty of advanced science and technology, Ryukoku University. In our laboratory, we are conducting research related to autonomous mobile robots and visible light communication. Autonomous mobile robots that work together with other robots are considered important. In addition, the mode of production in factories is changing from low-mix mass production to high-mix low-volume production.

Our research aims to explore various aspects of this evolving field, including pathfinding algorithms, and marker recognition techniques. In Section 2, we investigate the repulsion and attraction phenomena in addressing the stopping problem within the framework of potential fields methods[2]. Furthermore, Section 3 presents a proposal and evaluation concerning the optimal shape of reading cells, taking into account the directional blurring of AR markers[3] during movement. Finally, we summarize our findings and conclusions in the subsequent Section 4 of this paper.

2 Deadlock Problem by the Relationship between Repulsion and Attraction in Potential Field

2.1 Introduction

In recent years, autonomous mobile robots have emerged as a promising solution to address labor shortages across various industries, leading to a surge in research activities in this field. This research spans a wide array of areas, including sensor technology, image processing, and path planning.

Path selection, in particular, has garnered significant attention within autonomous mobile robot research. Path selection involves determining the most suitable path for an autonomous robot to navigate to its destination. One commonly utilized method for path selection is the potential field method.

In the potential field method, an attractive force function is defined at the destination, while a repulsive force function is defined at obstacles. The combined force of these functions determines the gradient vector, which guides the robot's movement. Specifically, the gradient vector of the repulsive function directs the robot away from obstacles, while the gradient vector of the attractive function guides it towards the destination. However, if the gradient vector consistently points towards a particular point, the robot may become trapped at that location.

Moreover, in this method, obstacles are treated as point sources of repulsion, with the repulsive force uniformly spreading from the center coordinates of the obstacle. Similarly, the attractive force spreads uniformly from the destination coordinates.

This paper explores the concept of "anchorage ease" by examining the interplay between repulsion and attraction forces while considering the shape of obstacles. By analyzing this relationship, the paper aims to enhance understanding of how obstacle shapes influence path planning and navigation strategies for autonomous mobile robots.

2.2 about effect by repulsion and attraction

Let the coordinates of the robot be (x_r, y_r), the coordinates of the i-th obstacle be (x_{o_i}, y_{o_i}), and the coordinates of the target position be (x_g, y_g). Let k_r and k_g represent the coefficients of repulsion and attraction, respectively. These coefficients are adjustable parameters. The expression for the potential function F_{r_i} for repulsion force is given by the equation: 1.

$$F_{r_i} = \frac{k_r}{\sqrt{(x_{o_i} - x_r)^2 + (yo_i - y_r)^2}} \tag{1}$$

The expression for the potential function F_g of the attractive force is given by Equation 2.

$$F_g = -\frac{k_g}{\sqrt{x_g - x_r)^2 + (y_g - y_r)^2}} \tag{2}$$

The expression for the function F representing the combined repulsive and attractive forces is given by Equation 3, where n is the number of obstacles.

$$F = (\sum_{i=1}^{n} F_{r_i}) + F_g \tag{3}$$

The gradient vector of the combined force, which represents the direction in which the robot is moving, is given by Equation 4.

$$-\nabla F = -\left[\frac{\partial F}{\partial x_r}, \frac{\partial F}{\partial y_r}\right] \tag{4}$$

To enhance the ease of anchorage, we modify the repulsion and attraction forces to align with the shape of the obstacle. Let (x_{e_i}, y_{e_i}) denote the point where the straight line intersects the obstacle when the coordinate points of the obstacle and the robot are connected by a straight line.

The expression for the length d_i from the coordinate point of the obstacle is given by Equation 5.

$$d_i = \sqrt{(x_{o_i} - x_{e_i})^2 + (y_{o_i} - y_{e_i})^2} \tag{5}$$

We modify the conventional repulsion and attraction potential functions by multiplying them by d_i. This adjustment results in greater repulsion at greater distances from the center of the obstacle to the edge, with a corresponding increase in attraction. Conversely, for portions of the obstacle where the distance from the center to the edge is small, both the repulsion and attraction forces are diminished accordingly.

gThe expression for the modified function of repulsion, denoted as F_{c_i}, is given by Equation 6.

$$F_{c_i} = F_r \times d_i = k_r \times \frac{\sqrt{(x_{o_i} - x_{e_i})^2 + (y_{o_i} - o_{e_i})^2}}{\sqrt{(x_{o_i} - x_r)^2 + (y_{o_i} - y_r)^2}} \tag{6}$$

The expression for the modified function of attraction, denoted as F_G, is given by Equation 7.

$$F_G = F_g \times d_i = -k_g \times \frac{\sqrt{(x_{o_i} - x_{e_i})^2 + (y_{o_i} - o_{e_i})^2}}{\sqrt{(x_g - x_r)^2 + (y_g - y_r)^2}} \tag{7}$$

F_{c_i} varies with both the distance to the obstacle and the distance to the edge of the obstacle, while F_G varies with the distance from the coordinates of the target position to the robot's coordinates.

The expression for F_p, the function representing the combined repulsive and attractive forces, is given by Equation 8.

$$F_p = \left(\sum_{i=1}^{n} F_{c_i}\right) + F_G \tag{8}$$

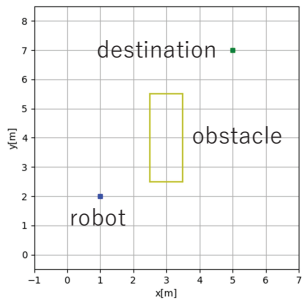

Fig. 1. The experimental environment

2.3 Experiment

Numerical simulations are conducted to analyze the robot's path using both the conventional potential field method and the modified potential field methods, focusing on the ease of stopping.

The experimental setup involves a rectangular obstacle with dimensions $x = 1$ meter and $y = 3$ meters located at coordinates $(3.0, 4.0)$ within an area bounded by $x = 6$ meters and $y = 8$ meters, as depicted in Figure 1. The origin is situated at the lower left corner.

In Case A of the experiment, we examine the differences between scenarios where the robot comes to a stop and where it continues moving. The initial position of the robot is set at $(1.0, 2.0)$ with a destination of $(4.0, 4.0)$. In Case B, the initial position is $(3.0, 1.0)$ with a destination of $(3.0, 7.0)$ for the robot. These experimental configurations aim to provide insights into the efficacy of the modified potential field methods in facilitating smoother and more efficient stopping of the robot under various initial and destination conditions.

The paths for Case A and Case B are illustrated in Figure 2 and Figure 3, respectively. In both figures: The orange line represents the path generated using the conventional potential field method. The blue line represents the path generated when both the repulsive and attractive forces are varied. The green line represents the path generated when only the repulsive force is varied. The red line represents the path generated when only the attractive force is varied. These color-coded paths provide a visual comparison of the trajectories resulting from different configurations of the potential field method.

In both Cases A and B, the robot failed to reach the target position and stopped when only the repulsive force was modified (green). In the experimental results, the system halted when only the repulsive force was adjusted. Figure 4 depicts the potential field for Case A with only the repulsive force modified. Observing the potential field, we notice that the repulsion force spreads out in a rectangular shape, while the attraction force spreads out in a circular manner. This leads to a constricted potential field where the repulsion force dominates. However, the potential field lacks a gradient vector that wraps around the obstacle, rendering it impossible for the robot to reach the target position. This

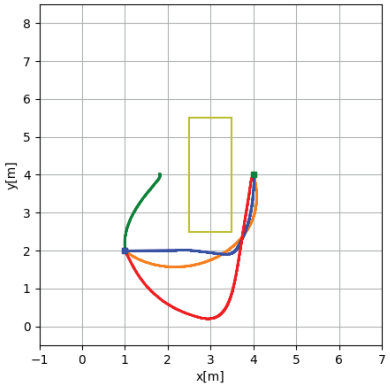

Fig. 2. Path of the robot in case A

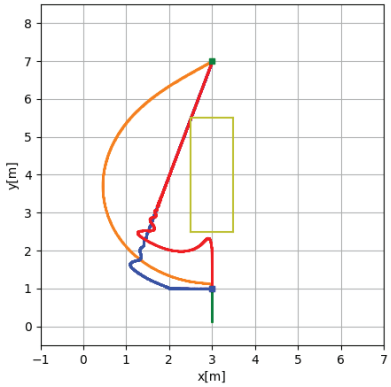

Fig. 3. The Path of the robot in case B

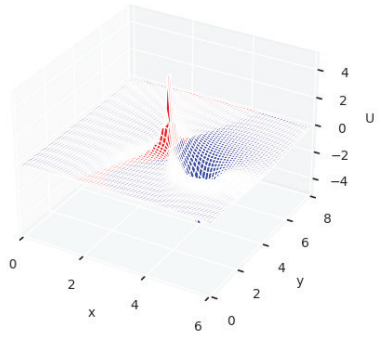

Fig. 4. Potential field when only the repulsion is changed

indicates that if the repulsive and attractive forces are in close proximity or if the repulsive force forms a regular circle, the potential field is less likely to be constricted by the attractive force, reducing the likelihood of the robot coming to a stop prematurely.

2.4 Conclusion

In this section, we have investigated the ease of stalls in potential field methods by varying the repulsive and attractive forces. In future research, we aim to explore the relationship between repulsion and attraction forces in scenarios involving multiple obstacles. Additionally, we plan to develop an algorithm for the potential field method that effectively prevents stalls from occurring. By further investigating these aspects, we aim to enhance the robustness and efficiency of potential field-based navigation methods for autonomous mobile robots.

3 Cell Shape Considerations Based on Robot Movement Direction

3.1 Introduction

Autonomous mobile robots operate independently, requiring precise self-position estimation to execute tasks accurately. ArUco markers are commonly employed for indoor self-position estimation, including in the RoboCup Logistics League (RCLL), a competition focusing on warehouse and factory automation. In RCLL, ArUco markers identify Modular Production Systems (MPS) and facilitate self-position estimation simultaneously.

However, capturing ArUco markers from a moving robot can lead to blurred images, impeding marker recognition. To address this challenge, we propose a recognition method for ArUco markers that accounts for motion blur direction.

Motion blur noise typically appears horizontally in captured images from moving robots. Therefore, when detecting ArUco markers, we selectively read only the region with a short width of the cell, rather than the entire cell. This approach reduces noise in the read cell, thereby enhancing the recognition rate of ArUco markers.

Experiments will be conducted at various robot speeds and distances from the markers to validate the effectiveness of the proposed method.

3.2 Recognition Method Considering Blurring

In essence, the moving robot exhibits forward/backward, horizontal, and rotational movements relative to the markers. As the robot moves back and forth, diagonal noise arises on captured markers, while horizontal noise occurs during horizontal movements or rotations. Additionally, vertical blurring can result from the robot's movement-induced vibration.

Considering that horizontal noise tends to be more pronounced than diagonal and vertical noise, the shape of the cell during marker detection is altered from a square to a elongated rectangle, as depicted in Figure 5. This adjustment effectively reduces the overall size of the cell, thereby accommodating the effects of blurring.

Subsequently, during the marker identification step, the number of black and white pixels within the rectangle is tallied to determine the cell's color.

3.3 Experiment

We conducted experiments to test our proposed recognition method, which considers the direction of blurring in ArUco markers, in order to assess the impact on the marker recognition rate.

As illustrated in Figure 6, the robot is maneuvered parallel to the marker, maintaining distances of 2 meters and 3 meters when positioned directly in front of the ArUco marker. The experiments were conducted at four different robot speeds: 0.3 m/s, 0.4 m/s, 0.5 m/s, and 0.6 m/s. The length of one side of the

Fig. 5. Cell for reading (blue box)

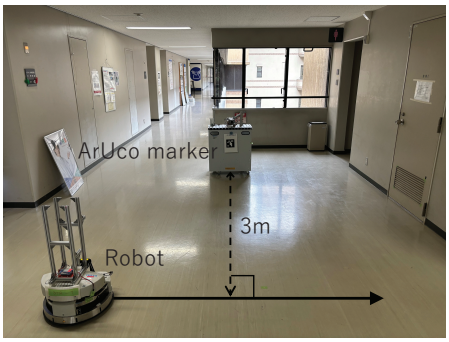

Fig. 6. An illustrated outline of experiment

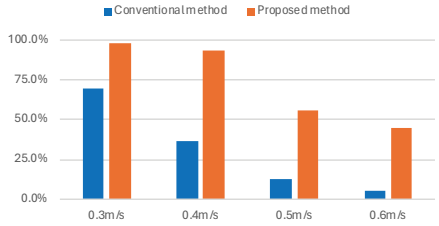

Fig. 7. Recognition ratio of conventional and proposed methods at 2 meters.

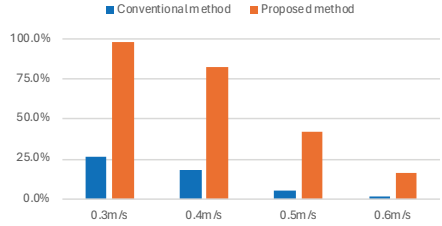

Fig. 8. Recognition ratio of conventional and proposed methods at 3 meters.

ArUco marker used is 13.5 cm. The shape of the cell to be read is adjusted to 0.8 for the vertical ratio and 0.5 for the horizontal ratio, relative to the original square shape.

The recognition rate is defined as the percentage of markers correctly identified from the captured images. The robot traveled three times in each direction (left and right), and the recognition rate was calculated based on a total of 6 captures. To assess the effectiveness of our proposed method, we compared the recognition rates obtained when the cell shape was 1:1 and 0.8:0.5.

The mobile robot utilized in the experiments is a Festo Robotino 3. The camera used for image capture is a HD Pro Webcam C920 manufactured by Logitech.

As depicted in the graphs in Figure 7 and Figure 8, the recognition rate exhibited improvement across all speeds when utilizing our proposed method. For the three scenarios where the recognition rate of the conventional method was less than 10%, the proposed method led to an approximately tenfold improvement in the recognition rate. Moreover, the recognition rates for the remaining data also demonstrated substantial enhancements. These findings suggest that our proposed method has the potential to expedite the successful estimation of self-location.

3.4 Conclusion

In this section, we introduce a novel cell shape for self-position estimation using ArUco markers during robot movement, considering the impact of noise induced by vibration. Comparison experiments between the conventional method and our proposed method revealed that our approach effectively mitigates the effects of motion blur and enhances the recognition rate of markers.

During the experiment, a consistent cell shape was utilized across all speeds. However, given that the degree of blurring is likely to vary based on factors such as the angle with the marker and the speed of the mobile robot, an area for future exploration involves implementing automatic cell deformation based on this information. This adaptive approach could further refine the accuracy and robustness of self-position estimation in dynamic environments.

4 Conclusion

We have been exploring the integration of autonomous mobile robots into various settings, including manufacturing and medical facilities, amidst the transition from high-mix low-volume production to factory production. Our research endeavors have encompassed investigating the selection criteria of computers for autonomous mobile robots and delving into pathfinding techniques.

Additionally, in our exploration of potential field methods, we have examined the ease of stopping by manipulating the repulsive and attractive forces. Notably, we observed that changes in the repulsive force resulted in the robot coming to a halt. As a next step, we plan to explore the relationship between repulsive and attractive forces in scenarios involving multiple obstacles and develop algorithms for potential field methods to prevent such unintended stops.

Moreover, we proposed a novel cell shape tailored to account for the effects of vibration-induced noise when estimating self-position using ArUco markers during robot movement. Experimental comparisons between our proposed method and conventional approaches revealed that our method effectively mitigated motion blur effects and improved marker recognition rates.

These collective research efforts signify our commitment to advancing the capabilities and reliability of autonomous mobile robots in real-world applications, with a focus on enhancing navigation, perception, and overall performance in dynamic environments.

References

1. BabyTigers - R, https://friede.elec.ryukoku.ac.jp/trac/lab/wiki/BabyTigers-R
2. Jen-Hui Chuang, and Narendra Ahuja: "An Analytically Tractable Potential Field Model of Free Space and Its Application in Obstacle Avoidance", IEEE TRANSACTIONS ON SYSTEMS,MAN,AND CYBERNETICS-PART B: CYBERNETICS, Vol.28, No.5, pp.729–736, 1998.
3. S. Garrido-Jurado, R. Munoz-Salinas, F. J. Madrid-Cuevas, and M. J. Marin-Jimenez: "Automatic generation and detection of highly reliable fiducial markers under occlusion", Pattern Recognition, 47(6),, pp.2280–2292, June 2014.